The soluble HIV-1 Vpu protein interacts with calmodulin in a Ca^{2+}-dependent manner

Olamide Ishola[1#], Md Majharul Islam[1#], Elaheh Hadadianpour[1], Peter P. Borbat[2], Elka R. Georgieva[1]*

[1]Department of Chemistry and Biochemistry, Texas Tech University, Lubbock, TX 79409

[2]Department of Chemistry and Chemical Biology, Cornell University, Ithaca, NY 14853.

* Corresponding author: Elka R. Georgieva, e-mail: elgeorgi@ttu.edu

[#]Equal contribution

ABSTRACT

The HIV-1-encoded membrane protein Vpu plays key roles in virus lifecycle. Our lab recently revealed a soluble form of Vpu, and we strived to determine its possible physiological function. Here, we provide solid experimental proof that soluble Vpu interacts with Ca^{2+}-bound calmodulin (Ca^{2+}-CaM). A putative CaM-binding motif in Vpu was predicted, but there was no experimental evidence of the Vpu-CaM association. We applied double electron electron-resonance (DEER) and protein spin labeling to detect the soluble Vpu-CaM complex. We found that soluble full-length and truncated C-terminal region of Vpu directly interact with Ca^{2+}-CaM. DEER results from the spin-labeled double cysteine mutant S39C/A103C of CaM showed that upon association with Vpu Ca^{2+}-CaM adopts a more closed conformation compared to those in the absence of Vpu. This restructuring is in agreement with previously observed Ca^{2+}-CaM association with cellular and other HIV-1 proteins. Our results indicate that soluble Vpu and CaM form an equimolar complex. DEER results from doubly spin-labeled at residues Q36C/I61C in Vpu C-terminal region suggest that Vpu's helices 2 and 3 move away from each other to facilitated CaM binding. These observations tell that under physiological conditions the soluble Vpu-CaM complex may provide Vpu with a trafficking pathway to membrane destination.

KEYWORDS: soluble HIV-1 Vpu protein, soluble Vpu-calmodulin interaction, DEER spectroscopy to study protein-protein complexes, protein conformational changes in protein-protein interaction

INTRODUCTION

Calmodulin (CaM) is a calcium sensor-protein playing key roles in cellular processes, e.g., it regulates the activity of enzymes and ion channels, affects the processes of development and cytoskeletal organization, etc.[1] In higher organisms, CaM is conserved, being ubiquitously expressed in high concentrations (>0.1% of total protein in the cells) and distributed to all cellular compartments[1, 2]. Extensive studies have identified and characterized several mechanisms of CaM interactions with its protein targets, which usually bind to CaM through electrostatic and hydrophobic interactions alike, both of which are provided by positive and hydrophobic residues in amphipathic helices[3]. Examples of target protein motifs interacting with Ca^{2+}-bound CaM are (x is any aa): the motif 1-10 [FILVW]xxxxxxxx[FILVW], the motif 1-5-10 [FILVW]xxx[FAILVW]xxxx[FILVW], the basic motif 1-5-10 [RK][RK][RK][FAILVW]xxx[FILV]xxxx[FILVW], etc. CaM interacts with some proteins in Ca^{2+}-independent manner. These proteins contain the following motifs: IQ [FILV]Qxxx[RK]Gxxx[RK]xx{FILVWY], IQ-like [FILV]Qxxx[RK]xxxxxxxx (which may require Ca^{2+} in some cases), IQ-2A [IVL]QxxxRxxxx[VL][KR]xW, etc.[4]

Besides the role in regulating cellular processes through protein-protein interactions, past studies have identified and characterized a group of HIV-1 encoded proteins, which recruit CaM to carry out their functions in the infected cells. It is well established that the association of CaM with HIV-1 encoded Nef, gp160, as well as the matrix (MA) domain of Gag proteins, are all essential for virus replication[5-9]. The HIV-1 Tat protein interaction with Ca^{2+}-bound CaM facilitates cell apoptosis[10]. It was also proposed that the HIV-1 Gag protein could utilize CaM for trafficking toward the plasma membrane to the site of virus assembly, as the CaM and Gag were co-localized in the cytosol[8]. In addition to the already characterized direct interactions between HIV-1 proteins and CaM, CaM-binding sites were predicted for most of the HIV-1-encoded 18 proteins[10]. These findings provide sufficient evidence that HIV-1 has developed efficient mechanisms to exploit the ubiquitous distribution of CaM in the cell.

This work is directed to investigate the interaction of the HIV-1 encoded protein Vpu with CaM. The putative CaM-binding motif (AIVVWSIVII<u>EYRKILRQRKIDRLI</u>) of Vpu with no strong homology to the well-characterized CaM-binding motifs was predicted earlier[10]. However, so far, no experimental data confirming the Vpu-CaM direct association have been reported. Vpu is a not

well understood non-structural protein, playing significant role in antagonizing cellular proteins, such as the immature CD4 receptor and tetherin, preventing them from delivery to the plasma membrane (PM) through early ubiquitination and degradation, and/or by deactivation of these proteins at the PM. In so doing, Vpu aids virus release[11, 12]. At a closer look, Vpu is a small protein having an N-terminal transmembrane (TM) helix (helix 1) followed by soluble helices 2 and 3. Helix 2 is amphipathic with the potential to associate with the membrane surface via electrostatic interactions, whereas helix 3, being mostly acidic, resides in the aqueous environment (Figures 1A and B)[13]. It was previously believed that Vpu is an exclusively membrane-resident protein, being found in membranes of endoplasmic reticulum (ER), Golgi and in the PM[13-16]. Recently, however, our lab discovered that Vpu can exist in a soluble oligomeric form[17, 18], whose physiological function we are poised to understand.

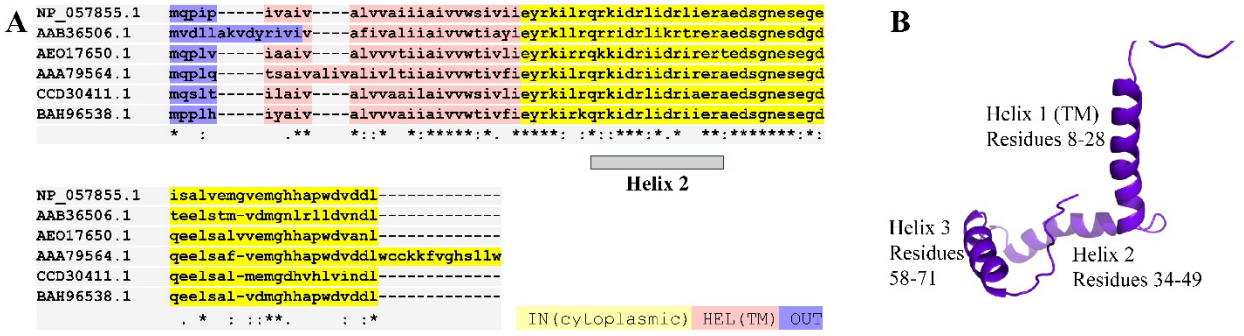

Figure 1. Amino acid (aa) sequence and membrane-bound structure of the HIV-1 Vpu protein: (**A**) The alignment of aa sequences of Vpu protein of randomly selected diverse HIV-1 strains, as follow: NP_057855.1 (strain for reference annotation); AAB36506.1 (an HIV-1 isolate of genetic subtype C); AEO17650.1 (HIV-1 sero-prevalent individual, subtype B); AAA79564.1 (isolate "cntrl 1", clone="3"; CCD30411.1 (group M, subgroup G); and BAH96538.1 (multidrug-resistant HIV-1 subtype B). In addition to the high conservation of the TM helix 1 (highlighted in tan), the composition of the loop between helix 1 and helix 2, and the helix 2 also demonstrate high sequence identity. The helix 2 is emphasized with gray bar under the aa sequences. (**B**) The solid-state NMR structure of full-length Vpu in lipid (PDB # 2N28) is shown with the helices 1, 2 and 3 labeled—helix 1 traverses membrane bilayer (not shown), whereas helix 2 is nearly parallel to the membrane surface. The unstructured loops between helices 1 and 2, and helices 2 and 3 are shown for clarity. The T-COFFEE software was used to align the Vpus' sequences, and PyMOL was used to visualize the ssNMR structure of Vpu.

To gain the insights into the cellular role of the soluble Vpu, we tested its interaction with CaM. We found that soluble Vpu associates with CaM in a Ca^{2+}-dependent manner, and upon this interaction CaM undergoes restructuring to adopt a more closed conformation resembling previously observed CaM associations with cellular and HIV-1 proteins[4, 10]. Our results land support to the model where soluble Vpu-CaM is an equimolar complex. We have also found that CaM interacts with the truncated C-terminal region of Vpu encompassing the residues 28-81 (EYRKILRQRKIDRLIDRLIERAEDSGNESEGEISALVEMGVEMGHHAPWDVDDL), which contains only a portion (underlined) of the putative CaM-binding site[10]. This may be indicative of Vpu having more than one binding site for CaM. In this work, we utilized protein engineering to generate spin labeled protein variants to obtain distance constraints using pulse dipolar electron spin resonance (ESR) spectroscopy, specifically double electron-electron resonance (aka DEER). The conformational changes in Vpu and CaM were probed by measuring the distances between the pairs of nitroxide spin labels linked to engineered cysteine residues in these proteins. We also have conducted amino acid sequence analysis to identify the plausible motifs in the C-terminal region of Vpu, which might contribute to the interaction with CaM.

A reasonable interpretation of our results could be a model that posits that under physiological conditions the soluble Vpu-CaM complex contributes to trafficking of Vpu towards its membrane destination, conceptually similar to proposed the Gag-CaM association[8]. Our findings aim to contribute to the understanding of HIV-1 Vpu protein interactions with the cellular components.

RESULTS

Analysis of the putative CaM-binding sites in the Vpu protein—localized in the TM helix 1, amphipathic helix 2, and the loop between them.

Because a putative CaM-binding motif in Vpu was proposed[10], we conducted further analysis of the Vpu amino acid (aa) sequence, to identify regions which might contain residues found in known motifs of CaM-binding proteins. We focused on the aa composition of the proposed CaM-binding region (Figure 2 A) but also expanded our search to account for residues in the helix 2 of Vpu (Figure 2 B). Like in other HIV-1-encoded CaM-binding proteins[8, 10], we could identify short sequences of residues in Vpu, which are identical to some of the canonical CaM-binding motifs[4,

[19]. However, Vpu's aa regions similar to more than one of these motifs (Figure 2 C) can clearly be recognized. Thus, the earlier proposed CaM-interacting region in Vpu has regions close to the patches of hydrophobic aa-s in the 1-8-14, 1-5-10 and IQ-like CaM-binding motifs. These hydrophobic residues are mostly located in the TM helix 1 of Vpu (Figure 2), i.e. IVVW sequence, highlighted in yellow in Figure 2 A. Whereas, the region of Vpu's helix 2 has greater resemblance with the 1-5-10 and IQ-like CaM-binding motifs due to the pairs of positive residues (RK – highlighted in magenta in Figure 2 A and B). Further, Vpu has a conserved Q (Gln) residue right before the helix 2 (highlighted in cyan in Figure 2 A and B), which is conceivably like the conserved Q residue in the IQ-like motif found in PEP-19 and RC3 proteins[20].

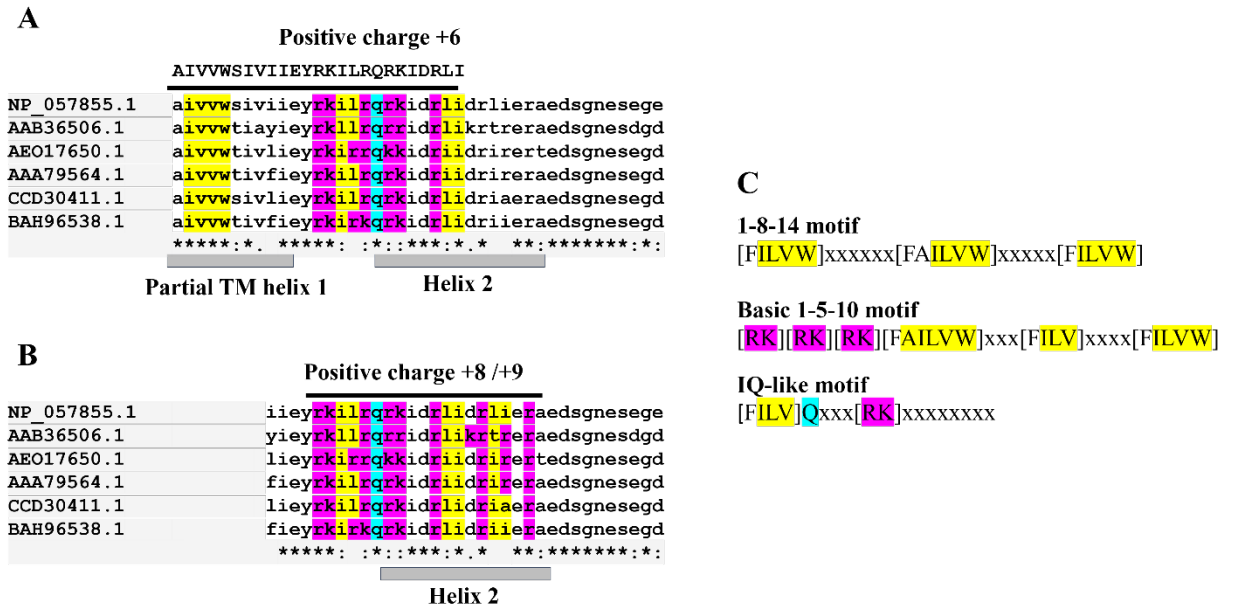

Figure 2. Analysis of the CaM-binding sites in the Vpu aa sequence. (**A**) The aligned Vpu aa sequences corresponding to the protein region containing the partial TM helix 1, helix 2 and the loops between helices 1/2 and 2/3 are shown. The aa sequence of the previously predicted CaM-binding motif and its positive charge (+6) are shown above the aligned aa sequences. (**B**) The aligned Vpu aa sequences corresponding to the protein region containing the helix 2 and the loops between helices 1/2 and 2/3 are shown. The positive charge of this aa region (+8 or +9, depending on the HIV-1 strain) is shown. For both (A) and (B) the Vpu aa are from the same HIV-1 staring shown in Figure 1. (**C**) The aa sequences of the common CaM-binding motifs, which have resemblance with the aa sequence of the putative Vpu's CaM-binding region are shown. The "x" in these sequences is an any aa. Proteins with these motives bind CaM in Ca^{2+}-dependent manner (except IQ-like motif, which could bind with and without Ca^{2+}). In all aa sequences, the basic residues, which are like those found in the basic 1-5-10 motif of CaM-binding proteins, are highlighted in magenta. The hydrophobic residues, which are like those found in the 1-8-14 and/or

1-14 motifs in CaM-binding proteins are highlighted in yellow. The conserved Gln (Q) residue in Vpu's aa sequences, which could be like the Gln residue found in the IQ-like motif of CaM-binding proteins is highlighted in cyan. This, it may well be that Vpu possesses a hybrid motif to associate with CaM via both electrostatic and hydrophobic interactions.

Consequently, careful aa sequence analysis suggests that Vpu possesses a hybrid CaM-binding sequence (motif) or possibly two distinct motifs, which interact with CaM via electrostatic and hydrophobic interactions. Furthermore, the basic 1-5-10 and 1-8-14 motifs associate with CaM in a Ca^{2+}-dependent manner[4, 19], which suggest that Vpu also interacts with Ca^{2+}-bound CaM.

The Ca^{2+}-bound CaM adopts more closed conformation upon binding to soluble Vpu

Because it was demonstrated that CaM plays a role in trafficking of HIV-1 proteins to membrane sites[7, 10], and that the HIV-1 protein Vpu has a CaM-binding sequence[10] (Figure 2) and can exists in a soluble form[17, 18], we asked whether soluble Vpu can directly interact with CaM. To this end, we studied the Vpu-CaM complex formation using highly-purified full-length (FL) and the truncated C-terminal region of Vpu (both constructs were fused to a SUMO tag, shown in Figures S1, S2 and S3), and CaM (Figure S4).

Our primary goal was to assess the conformational changes taking place in Ca^{2+}-bound CaM upon interaction with the soluble Vpu. For this purpose, we conducted DEER measurements of Ca^{2+}-bound CaM, doubly spin-labeled with MTS spin label (MTSL) at engineered cysteine residues S39C/A103C (Figure 2). Both residues, S39C and A103C, reside in the respective globular domains (N- and C-terminal lobes) separated by a long central helix in Ca^{2+}-bound CaM (Figure 2 A). DEER signals for this CaM variant were measured in CaM without Vpu added, and in the presence of unlabeled soluble SUMO-FL Vpu and SUMO- Vpu C-terminus at CaM-to-Vpu variant molar ratio of 1:0.75(0.8). All samples contained 1 mM Ca^{2+}. Therefore, we expected that CaM alone (without Vpu added) was predominantly in its well-defined extended Ca^{2+}-bound conformation[2]. This was confirmed by the DEER signal pattern with pronounced oscillations, yielding reconstructed distinct distance between the labeled residues, S39C and A103C (Figure 2 B, upper panel). The well-defined oscillating DEER signal was reconstructed to a narrow distance

distribution with a maximum at about 5.3 nm. This distance agrees well with the expected 4.1 nm distance between the C_β atoms of the residues S39 (S38) and A103 (A102) obtained from the crystal structure (Figure 2 A, upper panel). Note that our CaM construct was one residue longer than those whose crystal structures were solved and used in this study (PDB # 1EXR and PDB # 1IQ5) to compare the structure-predicted vs. experimental DEER distances. Still, the predicted DEER distance distribution using the molecular modeling software MMM[21] (Figure S5) is in agreement with the experimental distances from this study. This strongly suggest that the reason for the distance difference of5.3 nm measured by DEER vs 4.1 nm predicted based on C_β-C_β distances is due to the MTSL size and orientation. Furthermore, the DEER modulation depth (DEER signal amplitude at zero evolution time in the background-corrected "dipolar" signal) for this measurement corresponded to those expected for a pair of nitroxide spin labels in a fully labeled protein[22-25]. Expectedly, no distances were recorded by DEER in - Ca^{2+}-CaM singly spin-labeled at residue S39C (Figure S6). Therefore, these results suggest that only monomeric CaM in extended conformation was present in the sample.

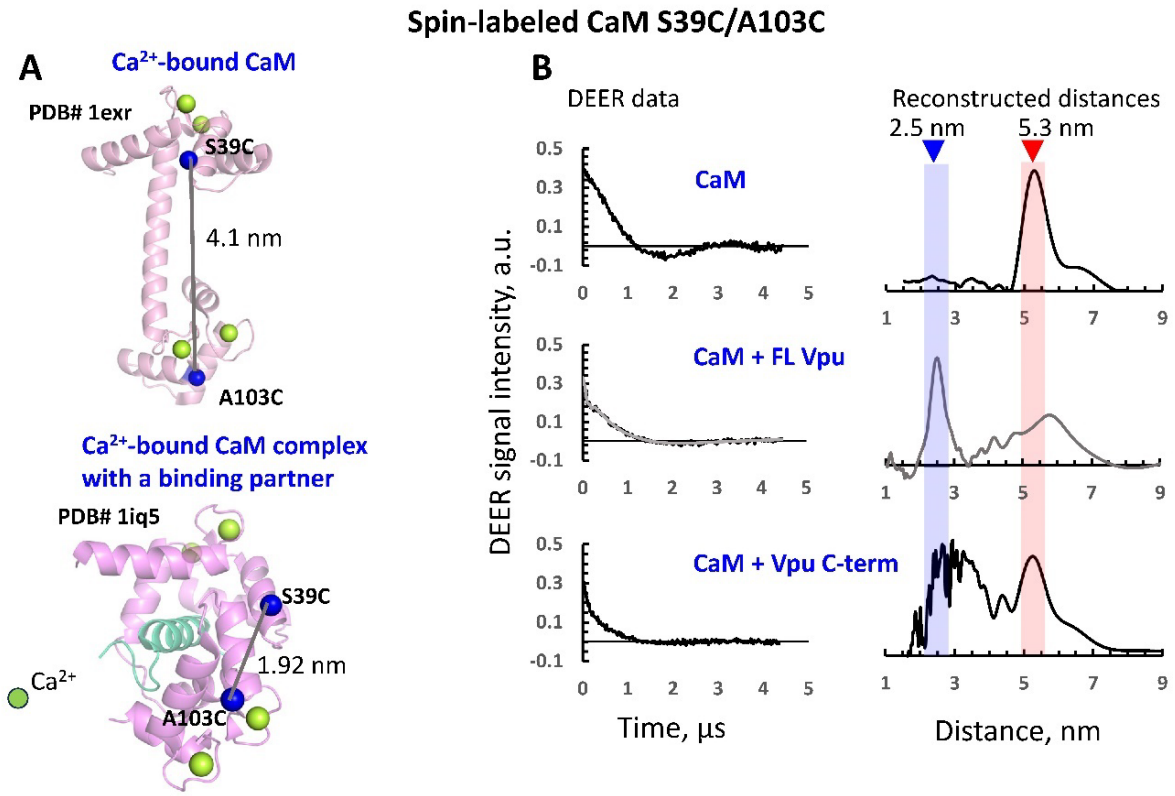

Figure 3. Ca^{2+}-bound CaM interacts with the FL Vpu and truncated C-terminal of Vpu. (A) The crystal structures of Ca^{2+}-bound CaM (PDB # 1EXR) and Ca^{2+}-bound CaM in the complex with a calmodulin dependent kinase fragment (cyan) (PDB # 1IQ5) illustrate extended and closed conformations, respectively. The C_β-atoms of residues S39 and A103 are shown as blue spheres. In the structures shown, these residues are S38 and A102, since these CaM forms are shorter by 1 aa compared to the one, which we used. The estimated C_β-C_β distances are also shown. (B) Baseline-corrected DEER data (left) accompanied by the reconstructed inter-spin label distances (right) for the following cases: (B, top) CaM doubly spin-labeled at residues S39C/A103C alone; (B, mid) CaM in the presence of excess of SUMO-FL Vpu; and (B, bottom) CaM with SUMO-C terminal region of Vpu. In the absence of these Vpu variants, a distinct DEER distance of 5.3 nm was obtained between MTSL labels at positions 39 and 103 in Ca^{2+}-bound CaM alone. However, with the addition of unlabeled Vpu variants shifts the average distance between residues 39/103 to a much shorter value of about 2.5 nm, thereby revealing a major restructuring of CaM. In the middle B-panel, reconstructed distance distribution is from the denoised DEER signal. This distance distribution is close to one obtained from original signal (Figure S6).

When soluble Vpu variants, i.e. the FL Vpu and its truncated C-terminal region were added to the CaM solution, substantial fraction of the DEER distances between CaM's spin-labeled residues S39C and A103C shifted into a short range (Figure 2 B, middle and lower panels, Figure S7), indicating the Vpu-CaM restructuring, obviously caused by formation of protein complex. The remaining distances of 5.3 nm indicated that not all CaM was bound to Vpu under the protein concentrations and the conditions of our experiment. We further conducted a quantitative analysis of the distance distributions by integrating the DEER distance distributions to find that a fraction of more than 50% of distances at 5.3 nm between spin-labeled residues S39C/A103C shifted to populations in the 4-2.5 nm range upon Ca^{2+}-CaM binding to Vpu (Figure S8). The newly appeared shorter distances are consistent with the closed conformation of Ca^{2+}-bound CaM when in a complex with a protein partner, exemplified with the calmodulin dependent kinase fragment (Figure 2 A, lower panel). In this conformation, the central helix of CaM is believed to transition to a less structured loop-like state or maybe one with a kink, allowing the two globular domains to come close to interact with the associated protein[26] (Figure 3 A). Furthermore, the binding of Vpu's variants did not lead to an increase in the DEER modulation depth, which would be possible if more than one CaM molecule would be bound to Vpu in an oligomer. This suggests that CaM bind soluble Vpu's as a monomer rather than a soluble-form Vpu's oligomer. The observed moderate

decrease of the DEER modulation depth, smeared signal oscillations, and broader distance distributions all could be explained by the increase of conformational heterogeneity of CaM due to the propensity of the central helix to break in its middle region.

The C-terminal region of Vpu undergoes restructuring upon binding to Ca^{2+}-CaM

To better understand the Vpu-CaM binding mechanism, we studied the spin-labeled double cysteine mutant Q36C/I61C of the Vpu C-terminal region (within the SUMO Vpu C-terminal construct) with cysteines located in the beginning of helix 2 and in helix 3 (Figure 4). We measured by DEER the distances between these residues in samples of Vpu C-terminus with and without Ca^{2+}-CaM present (Figure 4 A). Remarkably, upon the interaction of Vpu C-terminus with CaM, we observed a major shift in the distance between residues Q36C/I61C from about 2.5 nm well into the range of 3.5-5 nm (Figure 4 A, upper and lower panels, respectively), which suggest that the Vpu C-terminal region undergoes pronounced conformational rearrangements to accommodate the binding of CaM.

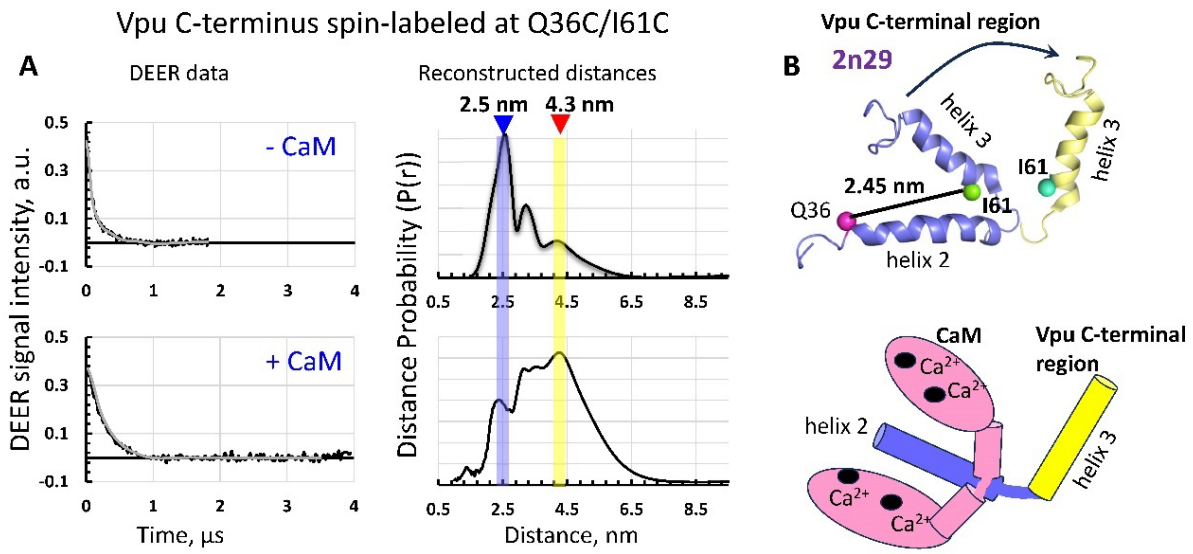

Figure 4. DEER on spin-labeled residues Q36C/I61C in the Vpu C-terminal indicate significant restructuring of this protein region upon binding to Ca^{2+}-CaM: (**A**) The baseline corrected DEER data (left) and reconstructed distances (right) for Vpu C-terminal spin-labeled at residues Q36C/I61C in the absence (upper panels) and presence (lower panels) of CaM. Significant shift in the main distances from about 2.5 nm to 3.5-5 nm was observed suggesting significant

restructuring in the Vpu C-terminus upon binding to CaM. (**B**) The proposed conformation rearrangements taking place in Vpu C-terminus upon binding of CaM—helix 3 moves further apart from helix 2. The ribbon-represented structure in blue in the upper panel is that of Vpu C-terminus, which was determined by NMR (PDB # 2N29).

It is worth mentioning that the DEER distance between residues Q36C/I61C in the Vpu C-terminal are very close to the distance of about 2.45 nm predicted based on the solution NMR structure of this protein region[16] (Figure 5 B), thus confirming the conformation with Vpu's helices 2 and 3 arranged in a hairpin. However, the binding of CaM to the helix 2 causes major restructuring in which the helix 3 of Vpu moves away from helix 2 (Figure 4 B), which resulted in much longer distances between residues Q31 and I61. Hence, through conducting these experiments, we were able to capture major conformational changes taking place in Vpu's C-terminal region upon Ca^{2+}-CaM-Vpu complex formation.

Careful examination of the DEER signals (Figure 4 A) shows that the DEER modulation depth in the sample of Vpu C-terminus without CaM is slightly greater than what is expected for a pair of interacting spin-labels (0.36 for the DEER settings in this work). This is most likely a result of partial Vpu C-terminus dimerization (Figure S9). However, these Vpu C-terminal dimers apparently dissociate upon binding to CaM because the DEER modulation depth decreases to the expected value in the presence of CaM. This is one more confirmation that Vpu and Ca^{2+}-CaM bind in equimolar ratio and suggest that the oligomers of Vpu C-terminus dissociate upon binding to Ca^{2+}-CaM.

Additional evidence about the direct interaction of the Vpu C-terminus and Ca^{2+}-CaM was obtained by measuring the DEER distances between the singly spin-labeled at residue R37C Vpu C-terminus and the CaM construct singly spin-labeled at S39C (Figure S10).

DISCUSSION

Regardless of the CaM-binding motif in the HIV-1 Vpu protein being predicted more than 10 years ago[10], no experimental evidence of such interaction has been provided. Moreover, the putative CaM-binding motif contains a substantial region coinciding with the Vpu TM helix 1 (Figure 2). Therefore, it looks puzzling how highly soluble CaM can associate with aa sequence region of Vpu, which is embedded in the membrane, in the case of membrane bound Vpu. Ca^{2+}-bound CaM was found to regulate several transmembrane proteins[4] , which however have CaM-binding sites in their soluble regions, e.g., connexin 45[27]. Our lab recently described a soluble form of Vpu[17, 18], which so far was not characterized in terms of physiological function in the framework of possible protein-protein interactions. Therefore, in this work, we sought to test if soluble Vpu can bind CaM. We further identified a more extended CaM-binding region in Vpu, encompassing residues in TM helix 1, helix 2 and the loop between helices 1 and 2 possessing the hybrid properties of more than one canonical CaM-binding motif, e.g., the 1-8-14, 1-5-10 and IQ-like motifs (Figure 2). The absence of a canonical CaM-binding motif in Vpu is not surprising, as this is common case for other HIV-1 CaM-binding proteins[7, 10]. What is more, it may well be that the Vpu has more than one CaM-binding site and, hypothetically, they are advantageous for the Vpu-CaM interactions. However, to determine this with high certainty, further detailed studies are needed.

With high certainty, however, this work provides solid experimental evidence that the recently identified soluble Vpu interacts with Ca^{2+}-bound CaM. This is based on our comprehensive DEER spectroscopy results on the interaction of spin-labeled CaM and Vpu proteins. The results strongly indicated that both Ca^{2+}-CaM and Vpu undergo conformational changes to conform to the specifics of the CaM-Vpu complex. Thus, upon binding to Vpu, the Ca^{2+}-bound CaM adopts more closed conformation based on the dramatic change of the DEER-derived distances between spin-labeled residues S39C and A103C, decreasing from 5.3 nm to 2.5 nm (Figure 3). This major restructuring is in line with previously observed conformational changes when Ca^{2+}-CaM interacts with cell's native proteins, where in the process the N- and C-terminal lobes of CaM come close to each other wrapping the binding region of the protein partner; the event facilitated by the unwinding of the central helix[4, 10]. In addition, we found that Vpu's C-terminal region undergoes substantial restructuring to facilitate the interaction with CaM by moving helix 3 further away from helix 2 (Figure 4).

Based on the aa sequence analysis and comparison with other CaM-binding protein motifs[3, 4], as well the DEER results from experiments on spin-labeled CaM and FL or truncated Vpu (Figures 3, and 4), we propose that Vpu's helix 2 and its flanking regions contribute to the Vpu-CaM interaction.

The results from this study also suggest that Vpu and CaM interact in equimolar ratio.

Here, we hypothesize that a possible physiological role of the soluble Vpu-CaM interaction could be one where Vpu utilizes CaM as a carrier for delivery to the membrane (Figure 6), as proposed for the HIV-1 Gag protein. Future studies may be necessary to clarify this hypothesis. It has been hypothesized that Vpu is synthesized at the ER membrane; however, this process has not been clearly described in the literature. Furthermore, the protein is found in the plasma membranes, and trans-Golgi network (TGN)[11, 28, 29], but its trafficking to these membranes is currently insufficiently understood. It may well be that the Vpu-CaM complex might take part in the process of Vpu distribution in the cells, particularly because the Vpu's CaM-binding motif(s) is highly conserved (Figure 2).

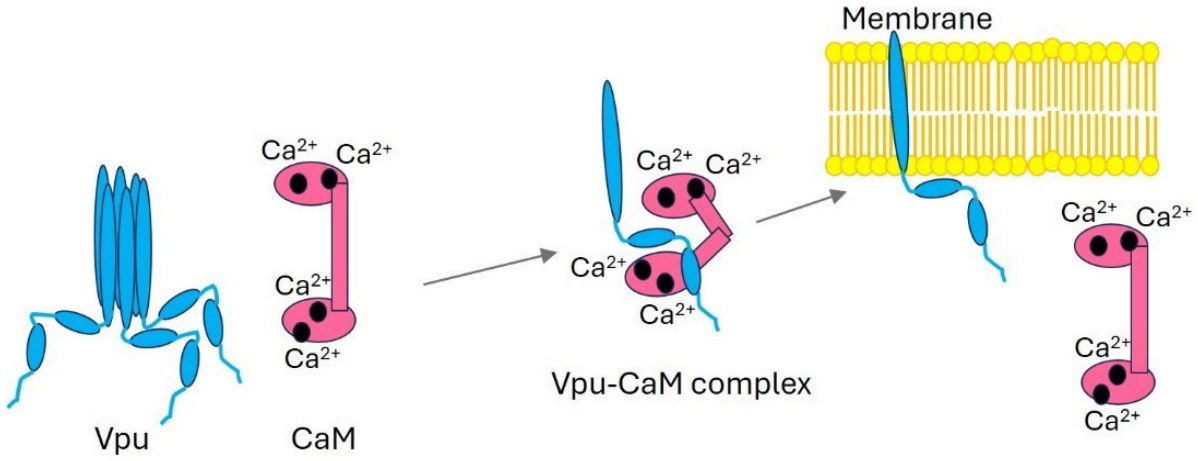

Figure 5. A hypothetical model of soluble Vpu-CaM physiological role: Soluble Vpu binds to Ca^{2+}-bound CaM in 1:1 stoichiometry to facilitate Vpu's trafficking to the membrane. Once Vpu is inserted into the membrane to adopt its functional state, CaM is released. The Ca^{2+} ions bound to CaM are shown as black circles.

Thus, this study provides new insight into the interaction of HIV1's Vpu with cellular components and expands our understanding of HIV-1's mechanisms in the host. Studies are being conducted in our lab to understand whether membrane-bound Vpu also interacts with CaM, or the membrane surface displaces CaM in a competitive interaction with Vpu's amphipathic helix 2. In ongoing studies, we also aim to comprehensively characterize the soluble Vpu-CaM complex and by detailed DEER mapping to identify with higher certainty the Vpu-CaM binding interface. This knowledge could be useful to informed design of Vpu inhibitors.

Our results experimentally detected the Vpu-CaM interaction, which adds to the lineage of the previously identified complexes of HIV-1 proteins with CaM. Thus, the growing evidence of the interactions of HIV-1 proteins with CaM might suggest that the virus efficiently utilizes CaM to adjust to the cell and control cellular physiology. Indeed, this might be a rational choice for HIV because of the ubiquitous localization and high concentration of CaM in the cell.

MATERIALS AND METHODS

Protein design, cloning, mutagenesis and expression

All fusion protein constructs, their cloning, and the protein mutations were designed in our lab; the DNA synthesis, cloning, and mutagenesis were conducted by GenScript, Inc.

Full-length (FL) Vpu was designed as a SUMO-Vpu-His_8 construct (referred here as SUMO-Vpu) having a SUMO tag at the N-terminus and polyhistidine purification tag at the C-terminus (Figure S2). The truncated C-terminal region of Vpu (residues 28-82) was designed as a His_8-SUMO-Vpu C-terminal construct (referred here as SUMO-Vpu C-terminus or SUMO-Vpu C-terminal region) (Figure S3). The protein solubilization using SUMO tag and other tags (e.g., MBP) was used in studies of proteins, including membrane proteins and viroporins[24, 30]. The wild-type (WT) Vpu, which we used, has no native cysteines, therefore the cysteine mutants used in this study were generated on the background of WT Vpu. The SUMO-Vpu had a cysteine residue generated through the mutation L42C (numbering in FL Vpu) which is in the Vpu helix 2, and a double cysteine mutant of the SUMO-Vpu C-terminus Q36C/I61C (numbering in FL Vpu) with cysteines in helices 2 and 3 was generated as well as a single cysteine mutant in the SUMO-Vpu C-terminus R37C. To verify that these point mutations do not affect Vpu folding, we compared the AlphaFold

models of the WT Vpu and the cysteine mutants—No measurable differences in the structures of WT vs. mutant were obtained (Figure S1).

Two CaM variants used in this study were the single cysteine mutant S39C and the double cysteine mutant S39C/A103C.

All proteins were cloned in pET15b *E. coli* expression vector at the Nco I and BamH I cloning sites, and the resulting plasmids carrying the gene for the protein of interest were transformed into chemically competent *E. coli* BL21(DE3) cells for protein expression. To express the proteins, *E. coli* colonies containing the plasmids carrying the SUMO-Vpu, SUMO-Vpu C-terminal and CaM were grown overnight on LB/agar/100 µg/ml ampicillin (Amp) plates at 37ºC. A single colony for each protein was selected to inoculate 200 ml of sterilized LB medium (Lennox) supplemented with 100 µg/ml Amp to produce the cell stock solution. The cells were grown overnight at 37 ºC and 180-200 rpm in an incubator-shaker. On the next day, 30 ml of the cell stock solution was transferred into each of larger flasks containing 2 l LB/100 µg/ml Amp and the cells were grown in the incubator shaker at 37 ºC and 180 rpm. After 2 h 30 min – 3h, when the OD of the cell solution reached 0.6-0.8, the temperature in the incubator-shaker was reduced to 14-18 ºC. After the desired temperature was reached, the protein expression under the control of T7 promoter was induced by adding IPTG (Isopropyl ß-D-1-thiogalactopyranoside) to a final concentration of 0.5-1 mM in each of the flacks. The protein expression was conducted overnight in the shaker-incubator at 14-18 ºC and 180 rpm for about 16-20 h.

Protein purification

All proteins were extracted from the cells using sonication and the soluble fractions were collected. Because all proteins (SUMO-Vpu, SUMO-Vpu C-terminus, and CaM) had His-tags, nickel affinity (Ni-affinity) chromatography was used in all purification protocols. The detailed protocols for the individual purification of each protein are provided below. The compounds used in the purifications were: NaCl (Thermo Scientific), HEPES (4-(2-hydroxyethyl)-1-piperazineethanesulfonic acid) (Sigma), TCEP (*tris*-(2-carboxyethyl)-phosphine) (Gold Biotechnology), chicken egg lysozyme (Roche), PMSF (phenyl-methylsulphonyl fluoride) (Gold Biotechnology), Urea (Sigma-Aldrich), Ni-NTA agarose resin (Qiagen), Imidazole (Sigma-Aldrich), glycerol (Thermo Scientific), Tris base (BioRad), sodium phosphate monobasic (Sigma-Aldrich), sodium phosphate

dibasic (Millipore-Sigma), DEAE resin (Cytiva), Phenyl Sepharose resin (Cytiva), $CaCl_2$ (Sigma), and β-DDM (n-Dodecyl-Beta-Maltoside) (Anatrace).

SUMO-Vpu purification: We harvested the cells by spinning them down in an Avanti J-15R centrifuge (Beckman coulter; JA-4.750 rotor) at 4,100 RPM (1,880×g) for 10 min at 4°C. We discarded the supernatant and collected and resuspended cell pellets in the resuspension buffer containing 20 mM HEPES pH 7.5 and 200 mM NaCl. Then, we added TCEP, chicken egg lysozyme, and PMSF to the resuspended cell solution to final concentrations of 200 μM, 0.5–0.6 mg/mL, and 1 mM, respectively. We then subjected this solution to sonication using a sonicator (U.S. solid ultrasonic processor) to break the cells open, and we separated the cell debris by centrifugation at 7,000 RPM (5,380×g) for 15 min in the same centrifuge (JA-10.100 rotor) at 4 °C. We collected the supernatant containing the soluble fraction of cell lysate and then using ultracentrifugation at 20,000 rpm (27,400×g) for 1 h in an Optima XE-90 ultracentrifuge (Beckman Coulter) in 70.1Ti rotor at 4 °C we span down most of the membranes. The supernatant was collected and urea was added to final 8 M on stirring mode. Then, we added to the protein solution Imidazole (Im) to 20 mM final concentration as a background to prevent the binding of impurities to the Ni-NTA resin.

We utilized Ni-affinity chromatography to purify the SUMO-Vpu protein. For Ni-affinity purification, we incubated Ni-NTA agarose resin (1.5 ml/1 L cell culture) at room temperature (RT) for 1–1.5 h. Afterward, we transferred Ni-NTA agarose resin bound with protein to a gravity column and discarded flow-through containing the unbound material. Then, to elute most of the weakly bound protein impurities, we washed the column first with 12 resin volumes of buffer A containing 50 mM of sodium phosphate buffer, pH 7.4; 500 mM of NaCl, and 5 % (w/v) glycerol supplemented with 70 mM Im, 8 M Urea, 200 μM TCEP. Next, the resin was washed with 3 volumes of buffer A supplemented with 85 mM of Im, 8 M Urea, 200 uM TCEP to the column. Afterward, we eluted the SUMO-Vpu protein using 2.5 resin volumes of buffer A supplemented with 320 mM Im, 8 M Urea, 200 μM TCEP. Next, we concentrated the protein at 3,900 RPM (1,700×g) in 10-kDa MWCO centrifugal filters (Amicon®) at 4 °C-10 °C. We gradually refolded the protein by washing out the Urea with buffer A supplemented with 1 mM β-DDM. Prior to binding experiments with CaM, the SUMO-Vpu buffer was exchanged with a β-DDM- and EDTA-free buffer. We measured the protein concentration using nanodrop spectrophotometer

(Thermo Scientific) using the calculated extinction coefficient of 13,980 $M^{-1}cm^{-1}$ and absorbance at 280 nm. We used this highly pure protein in further experiments.

SUMO-Vpu C-terminus purification: The cells were harvested by centrifugation in an Avanti J-15R centrifuge (Beckman coulter; JA-4.750 rotor) at 4,100 RPM (1,880×g) for 10 min at 4°C. The cell pellets were resuspended in a buffer A containing 20 mM Tris/HCl pH 7.5, 500 mM NaCl, 5% glycerol. To the cell solution, PMSF, lysozyme, and TCEP to final concentrations of 1 mM, 1 mg/ml and 200 µM, respectively, were added. The unbroken cells and cell debris were removed by centrifugation at 7,000 RPM (5,380 ×g) for 15 min in the same centrifuge (JA-10.100 rotor) at 4 °C. The supernatant containing the SUMO-Vpu C-terminal protein was transferred into 27 ml ultracentrifuge tubes and the membranes plus the heavy impurities were spun down in a Beckman ultracentrifuge Optima XE-90 at 40,000 rpm (110,000×g) for 1 hour at 4 °C. The supernatant containing SUMO-Vpu C-terminus was subjected to Ni-affinity chromatography using the Ni-NTA resin. To this end, the preequilibrated with buffer A Ni-NTA resin was mixed with the soluble protein fraction for 1h at 4ºC under constant agitation. Thereafter, the Ni-NTA resin with bound protein was washed with 10 resin volumes of buffer A supplemented with 50 mM Im to remove weakly-bound protein impurities. The SUMO-Vpu C-terminal protein was eluted with 3 resin volumes of buffer A supplemented with 300 mM Im.

To increase protein purity, additional purification step using ion exchange chromatography was added. Since the SUMO-Vpu C-terminus is negatively charged at pH 7.4, we bound the protein to DEAE-Sepharose ion-exchange resin for 1h at 4 ºC. Prior to this, the Im-eluted protein was desalted to remove the Im and NaCl completely. Removing NaCl allows protein to bind positively-charged DEAE resin. To do so, the buffer was exchanged to 20 mM Tris/HCl pH 7.5, 1 mM EDTA, 5% glycerol (w/v) (buffer B). The protein impurities bound to the DEAE-Sepharose resin were removed using a stepwise NaCl concentration gradient: 2-5 resin volumes of 20 mM and 55 mM NaCl in buffer B were used. Thereafter, the SUMO-Vpu C-terminal protein was eluted using buffer B supplemented with 300 mM NaCl. Protein purity was assessed via SDS-PAGE and WB (Figure S3). Protein concentration was estimated using the calculated extinction coefficient of 8,604 M^{-1} cm^{-1} for the absorbance at 280 nm.

CaM purification: We harvested the cells by spinning them down in an Avanti J-15R centrifuge at 4,100 RPM for 12 min at 4 ºC. We discarded the supernatant and collected and resuspended the

cell pellets in the resuspension buffer A containing 20 mM Tris pH 7.4, 150 mM NaCl, 200 µM TCEP, and 5% glycerol. Then, we added chicken egg lysozyme and PMSF to the resuspended cell solution to the final concentrations of 0.4 mg/mL and 1 mM, respectively. We then broke the cells open using the sonicator. We separated the cell debris and unbroken cells by centrifugation at 7,000 RPM (5,380 ×g) for 15 min in the same centrifuge (JA-10.100 rotor) at 4 °C. We transferred the supernatant to 27 ml ultracentrifuge tubes and span down the membranes in an Optima XE-90 Beckman ultracentrifuge at 40,000 RPM (110,000×g) for 1h at 4 ºC. We collected the supernatant containing the soluble CaM. We purified the CaM protein using Ni-affinity chromatography: We incubated the protein solution with Ni-NTA agarose resin (1.5 ml/1 L cell culture) under constant agitation at 4 °C for 1h. Afterward, we transferred Ni-NTA agarose resin bound with protein to a gravity column and discarded the flow-through fraction containing the unbound material. Then, to elute most of the weakly bound protein impurities, we washed the column with 10 resin volumes of buffer A containing 20 mM Tris pH 7.4, 150 mM NaCl, 200 µM TCEP, 5% glycerol (w/v), supplemented with 65 mM Im. Subsequently, we added 3 resin volumes of buffer A containing 20 mM Tris pH 7.4, 150 mM NaCl, 200 µM TCEP, 5% glycerol (w/v), supplemented with 320 mM Im to the column to elute the bound CaM. To obtain highly pure CaM, we further subjected the Ni-affinity purified protein to Phenyl Sepharose purification, taking advantage of the exposed hydrophobic residues in Ca^{2+}-bound CaM[31]. To this end, we exchanged the buffer of the Ni-affinity purified CaM with a buffer B made of 20 mM Tris, pH 7.4; 150 mM NaCl, 200 µM TCEP, 5% glycerol (w/v), and 5 mM $CaCl_2$. We bound this protein to the preequilibrated with buffer B Phenyl Sepharose 6 fast flow (High Sub) resin at 4 ºC for 1h under constant agitation. Afterward, we transferred the Phenyl Sepharose 6 fast flow (High Sub) resin with bound protein to a gravity column and discarded the flow-through fraction containing the unbound material. Then we washed the resin with bound CaM with 10 resin volume of buffer B. Next, we eluted the bound CaM with 3-resin volumes of buffer C containing 20 mM Tris, pH 7.4; 150 mM NaCl; 200 µM TCEP; 5% glycerol, and 10 mM EGTA. We collected the eluted CaM and concentrated it at 3,900 RPM in 10-kDa MWCO centrifugal filters at 4 °C. We measured protein concentration with the nanodrop spectrophotometer using the calculated extinction coefficient of 2,980 M^{-1} cm^{-1}. The protein purity was confirmed using SDS-PAGE and Western Blotting (Figure S4). We used this highly pure protein in further experiments.

Protein spin labeling

The SUMO-Vpu single cysteine mutant L42C (the cysteine is in the Vpu polypeptide, and the numbering is in FL Vpu) and CaM single S39C and double S39C/A103C cysteine mutants were labeled with the MTS spin label (MTSL). MTSL is widely used paramagnetic tag in protein ESR studies[32-34]. The SUMO-Vpu C-terminal single R37C and double Q36C/I61C cysteine mutants were labeled with the 3-(2-Iodoacetamido)-PROXYL spin label (ISL) because when MTSL was added the SUMO-Vpu C-term protein precipitated out, like other viral proteins studied previously[35]. Note that the cysteines are those of the Vpu polypeptide and the numbering corresponds to FL Vpu.

SUMO-Vpu C-terminal region labeling: Prior to labeling, the buffer of the purified R37C and Q36C/I61C mutants was exchanged to 20 mM Tris/HCl pH 7.9, 150 mM NaCl, 5% (w/v) glycerol and 50 mM TCEP. Then an aliquot of 50 mM ISL stock solution in acetonitrile was added to the protein solutions for the final protein-to-ISL molar ratio of 1:10. The reaction was allowed to proceed for 3-4 h at 22 ºC under constant agitation. Unreacted ASL was removed by washing protein solution with a buffer containing Tris/HCl pH 7.4, 150 mM NaCl, 1 mM $CaCl_2$ and 5% (w/v) glycerol.

CaM labeling: Prior to spin labeling, the buffer of the purified CaM S39C and S39C/A103 cysteine mutants was exchanged to 20 mM Tris, pH 7.4; 150 mM NaCl; 5% glycerol; and 1 mM $CaCl_2$. The CaM concertation was about 100 µM. Then, and aliquot of the 100 mM MTSL stock solution in acetonitrile was added to the CaM mutant solution for the final 1:10 (or 15) CaM:MTSL molar ratio. The reaction was allowed to proceed for 2h 30 min at 22 ºC and then overnight at 4ºC. The unreacted label was removed by washing the protein solution in a 5 kDa MWCO concentrator with a buffer containing 20 mM Tris/HCl pH 7.4; 150 mM NaCl, 5% glycerol (w/v), and 1 mM $CaCl_2$. Finaly, the buffer of the spin-labeled S39C/A103C mutant was exchanged to 20 mM Tris/HCl, 150 mM NaCl, 1 mM $CaCl_2$ and about 80% D_2O instead of H_2O to increase the MTSL phase relaxation times, allowing us to measure longer distances by DEER spectroscopy (DEER for short) [36, 37].

Preparation of samples for DEER spectroscopy

The following samples were prepared for DEER measurements: (i) Ca^{2+}-CaM spin-labeled at residues S39C/A103C at 30 µM and 40 µM concertation in buffer containing about 80% D_2O/

about 20 % H_2O. (ii) 30 μM Ca^{2+}-CaM spin-labeled at residues S39C/A103C mixed with 40 μM of SUMO-FL Vpu L42C mutant non-labeled. The final sample contained about 50% D_2O. (iii) 30 μM/25 μ Ca^{2+}-CaM spin-labeled at residues S39C/A103C mixed with 35 μM/35 μM of SUMO-Vpu C-terminal R37C mutant non-labeled. The final samples contained about 50% D_2O. (iv) 30 μM Ca^{2+}-CaM spin-labeled at residue S39C. (v) 40 μM Ca^{2+}-CaM spin-labeled at residues S39C mixed with 40 μM SUMO-FL Vpu spin-labeled at residue R37C. (vi) 30 μM SUMO-Vpu C-terminal spin-labeled at residues Q36C/I61C. (vii) 30 μM SUMO-Vpu C-terminal spin-labeled at residues Q36C/I61C mixed with 50 μM non-labeled Ca^{2+}-CaM S39C mutant.

All samples contained 20-25% (w/v) glycerol or glycerol-D8 as cryoprotectant and all buffers contained 1 mM $CaCl_2$.

DEER spectroscopy experiments and data processing

DEER measurements were carried out at ACERT, Cornell University. The measurements were conducted at 60 K using a home-built Ku-band pulse ESR spectrometer operating at MW frequency band around 17.3 GHz [38, 39]. The sample solutions were placed into fused silica 2.0 mm I.D. Vitrotubes® capillaries and flash frozen for the measurements. A standard 4-pulse DEER experiment [40] setup was the same as used previously[25]. Briefly, for electron spin-echo detection a π/2-π-π pulse sequence with 32-ns π-pulse width was applied at the low-field edge of the nitroxide spectrum and 16-ns π-pulse at a 70 MHz lower frequency pumped at the spectrum central peak. A 32-step phase cycle[41] was applied for suppressing unwanted coherence pathways contributing to the signal and removing some instrumental artifacts leaving only small contributions from the three unremovable dipolar pathways endemic to the 4-pulse DEER sequence. Such contributions caused by dipolar coupling are phase-independent and cannot be removed by phase cycling[42]. Nuclear electron spin-echo envelope modulation (ESEEM) caused by surrounding protons was suppressed by summing up four data traces recorded for each timing point in sequential measurements in which initial pulse separations and the start time of detection were advanced in 9.5 ns steps in subsequent measurements, that is by quarter period of the 26.2-MHz nuclear Zeeman frequency of protons at 615 mT for 17.3 GHz working frequency[43]. For samples that contained deuterated buffers, this usually was unnecessary. The recorded DEER signals were background corrected using log-linear baseline[25], e.g. as shown in Figure S11. The inter-spin distances between the labels were reconstructed using Tikhonov regularization software[44] and/or

SVD as needed. The reconstructions were stable and often similar with both methods, but the second was preferred. In this method some of the original DEER signals were denoised[45] to facilitate sf-SVD reconstructions[46] leading to generally more stable distance distributions, $P(r)$'s, as a matter of a larger number of singular values. The obtained distances are similar when reconstructed from the DEER signal before and after denoising (Figure 3 and Figure S8), but sf-SVD result appears more robust. Note that in these methods no positivity constraint is used, therefore some reconstructed $P(r)$'s may contain small negative contributions. For example, residual ESEEM contributing to the signal in the opposite phase will faithfully reconstruct as a narrow negative peak in expected position and can be manually removed, if needed. Orientation selection, multi-spin effects and other minor artifacts aside of "ghost" lines could also produce negative contributions that may help recognize their origin and mitigate the reconstruction. The positivity constraint, however, like in MEM[47] seeded by truncated L-curve Tikhonov distributions converts these artifacts into forced $P(r)$ distortions.

AUTHOR CONTRIBUTION

OI: experiment, data analysis, figures; MMI: experiment, data analysis, figures; EH: experiment, figures; PPB: experimental design, experiment, data analysis and interpretation, figures; ERG: conception, experimental design, experiment, data analysis and interpretation, drafting the manuscript, figures and artwork, project oversight. All Authors approved the final version of the manuscript

FUNDING

The work was supported by Gilead Research Scholar in HIV Award and TTU start-up funds (to ERG). The ACERT (Cornell University) is supported by an NIH grant 1R24GM146107.

REFERENCES

(1) Chin, D.; Means, A. R. Calmodulin: a prototypical calcium sensor. *Trends Cell Biol* **2000**, *10* (8), 322-328. DOI: 10.1016/s0962-8924(00)01800-6 From NLM Medline.

(2) Yang, C. F.; Tsai, W. C. Calmodulin: The switch button of calcium signaling. *Tzu Chi Med J* **2022**, *34* (1), 15-22. DOI: 10.4103/tcmj.tcmj_285_20 From NLM PubMed-not-MEDLINE.

(3) O'Neil, K. T.; DeGrado, W. F. How calmodulin binds its targets: sequence independent recognition of amphiphilic alpha-helices. *Trends Biochem Sci* **1990**, *15* (2), 59-64. DOI: 10.1016/0968-0004(90)90177-d From NLM Medline.

(4) Andrews, C.; Xu, Y.; Kirberger, M.; Yang, J. J. Structural Aspects and Prediction of Calmodulin-Binding Proteins. *Int J Mol Sci* **2020**, *22* (1). DOI: 10.3390/ijms22010308 From NLM Medline.

(5) Miller, M. A.; Mietzner, T. A.; Cloyd, M. W.; Robey, W. G.; Montelaro, R. C. Identification of a calmodulin-binding and inhibitory peptide domain in the HIV-1 transmembrane glycoprotein. *AIDS Res Hum Retroviruses* **1993**, *9* (11), 1057-1066. DOI: 10.1089/aid.1993.9.1057 From NLM Medline.

(6) Sham, S. W.; McDonald, J. M.; Micoli, K. J.; Krishna, N. R. Solution structure of a calmodulin-binding domain in the carboxy-terminal region of HIV type 1 gp160. *AIDS Res Hum Retroviruses* **2008**, *24* (4), 607-616. DOI: 10.1089/aid.2007.0202 From NLM Medline.

(7) Radding, W.; Williams, J. P.; McKenna, M. A.; Tummala, R.; Hunter, E.; Tytler, E. M.; McDonald, J. M. Calmodulin and HIV type 1: interactions with Gag and Gag products. *AIDS Res Hum Retroviruses* **2000**, *16* (15), 1519-1525. DOI: 10.1089/088922200750006047 From NLM Medline.

(8) Ghanam, R. H.; Fernandez, T. F.; Fledderman, E. L.; Saad, J. S. Binding of calmodulin to the HIV-1 matrix protein triggers myristate exposure. *J Biol Chem* **2010**, *285* (53), 41911-41920. DOI: 10.1074/jbc.M110.179093 From NLM Medline.

(9) Vlach, J.; Samal, A. B.; Saad, J. S. Solution structure of calmodulin bound to the binding domain of the HIV-1 matrix protein. *J Biol Chem* **2014**, *289* (12), 8697-8705. DOI: 10.1074/jbc.M113.543694 From NLM Medline.

(10) McQueen, P.; Donald, L. J.; Vo, T. N.; Nguyen, D. H.; Griffiths, H.; Shojania, S.; Standing, K. G.; O'Neil, J. D. Tat peptide-calmodulin binding studies and bioinformatics of HIV-1 protein-calmodulin interactions. *Proteins* **2011**, *79* (7), 2233-2246. DOI: 10.1002/prot.23048 From NLM Medline.

(11) Khan, N.; Geiger, J. D. Role of Viral Protein U (Vpu) in HIV-1 Infection and Pathogenesis. *Viruses* **2021**, *13* (8). DOI: 10.3390/v13081466 From NLM Medline.

(12) Dube, M.; Bego, M. G.; Paquay, C.; Cohen, E. A. Modulation of HIV-1-host interaction: role of the Vpu accessory protein. *Retrovirology* **2010**, *7*, 114. DOI: 10.1186/1742-4690-7-114 From NLM Medline.

(13) Ma, C.; Marassi, F. M.; Jones, D. H.; Straus, S. K.; Bour, S.; Strebel, K.; Schubert, U.; Oblatt-Montal, M.; Montal, M.; Opella, S. J. Expression, purification, and activities of full-length and truncated versions of the integral membrane protein Vpu from HIV-1. *Protein Sci* **2002**, *11* (3), 546-557. DOI: 10.1110/ps.37302.

(14) Sharpe, S.; Yau, W. M.; Tycko, R. Structure and dynamics of the HIV-1 Vpu transmembrane domain revealed by solid-state NMR with magic-angle spinning. *Biochemistry* **2006**, *45* (3), 918-933. DOI: 10.1021/bi051766k From NLM Medline.

(15) Strebel, K.; Klimkait, T.; Martin, M. A. A novel gene of HIV-1, vpu, and its 16-kilodalton product. *Science* **1988**, *241* (4870), 1221-1223. DOI: 10.1126/science.3261888.

(16) Zhang, H.; Lin, E. C.; Das, B. B.; Tian, Y.; Opella, S. J. Structural determination of virus protein U from HIV-1 by NMR in membrane environments. *Biochim Biophys Acta* **2015**, *1848* (11 Pt A), 3007-3018. DOI: 10.1016/j.bbamem.2015.09.008 From NLM Medline.

(17) Majeed, S.; Adetuyi, O.; Borbat, P. P.; Majharul Islam, M.; Ishola, O.; Zhao, B.; Georgieva, E. R. Insights into the oligomeric structure of the HIV-1 Vpu protein. *J Struct Biol* **2023**, *215* (1), 107943. DOI: 10.1016/j.jsb.2023.107943 From NLM Medline.

(18) Majeed, S.; Dang, L.; Islam, M. M.; Ishola, O.; Borbat, P. P.; Ludtke, S. J.; Georgieva, E. R. HIV-1 Vpu protein forms stable oligomers in aqueous solution via its transmembrane domain self-association. *Sci Rep* **2023**, *13* (1), 14691. DOI: 10.1038/s41598-023-41873-0 From NLM Medline.

(19) Rhoads, A. R.; Friedberg, F. Sequence motifs for calmodulin recognition. *FASEB J* **1997**, *11* (5), 331-340. DOI: 10.1096/fasebj.11.5.9141499 From NLM Medline.

(20) Putkey, J. A.; Kleerekoper, Q.; Gaertner, T. R.; Waxham, M. N. A new role for IQ motif proteins in regulating calmodulin function. *J Biol Chem* **2003**, *278* (50), 49667-49670. DOI: 10.1074/jbc.C300372200 From NLM Medline.

(21) Jeschke, G. MMM: A toolbox for integrative structure modeling. *Protein Sci* **2018**, *27* (1), 76-85. DOI: 10.1002/pro.3269 From NLM Medline.

(22) Georgieva, E. R.; Borbat, P. P.; Ginter, C.; Freed, J. H.; Boudker, O. Conformational ensemble of the sodium-coupled aspartate transporter. *Nat Struct Mol Biol* **2013**, *20* (2), 215-221. DOI: 10.1038/nsmb.2494 From NLM Medline.

(23) Georgieva, E. R.; Roy, A. S.; Grigoryants, V. M.; Borbat, P. P.; Earle, K. A.; Scholes, C. P.; Freed, J. H. Effect of freezing conditions on distances and their distributions derived from Double Electron Electron Resonance (DEER): a study of doubly-spin-labeled T4 lysozyme. *J Magn Reson* **2012**, *216*, 69-77. DOI: 10.1016/j.jmr.2012.01.004 From NLM Medline.

(24) Jeschke, G.; Sajid, M.; Schulte, M.; Godt, A. Three-spin correlations in double electron–electron resonance. *Physical chemistry chemical physics* **2009**, *11* (31), 6580-6591.

(25) Sanders, G.; Borbat, P. P.; Georgieva, E. R. Conformations of influenza A M2 protein in DOPC/DOPS and E. coli native lipids and proteins. *Biophys J* **2024**, *123* (16), 2584-2593. DOI: 10.1016/j.bpj.2024.06.025 From NLM Medline.

(26) Kurokawa, H.; Osawa, M.; Kurihara, H.; Katayama, N.; Tokumitsu, H.; Swindells, M. B.; Kainosho, M.; Ikura, M. Target-induced conformational adaptation of calmodulin revealed by the crystal structure of a complex with nematode Ca(2+)/calmodulin-dependent kinase kinase peptide. *J Mol Biol* **2001**, *312* (1), 59-68. DOI: 10.1006/jmbi.2001.4822 From NLM Medline.

(27) Zou, J.; Salarian, M.; Chen, Y.; Zhuo, Y.; Brown, N. E.; Hepler, J. R.; Yang, J. J. Direct visualization of interaction between calmodulin and connexin45. *Biochem J* **2017**, *474* (24), 4035-4051. DOI: 10.1042/BCJ20170426 From NLM Medline.

(28) Pacyniak, E.; Gomez, M. L.; Gomez, L. M.; Mulcahy, E. R.; Jackson, M.; Hout, D. R.; Wisdom, B. J.; Stephens, E. B. Identification of a region within the cytoplasmic domain of the subtype B Vpu protein of human immunodeficiency virus type 1 (HIV-1) that is responsible for retention in the golgi complex and its absence in the Vpu protein from a subtype C HIV-1. *AIDS Res Hum Retroviruses* **2005**, *21* (5), 379-394. DOI: 10.1089/aid.2005.21.379 From NLM Medline.

(29) Ruiz, A.; Hill, M. S.; Schmitt, K.; Guatelli, J.; Stephens, E. B. Requirements of the membrane proximal tyrosine and dileucine-based sorting signals for efficient transport of the subtype C Vpu protein to the plasma membrane and in virus release. *Virology* **2008**, *378* (1), 58-68. DOI: 10.1016/j.virol.2008.05.022 From NLM Medline.

(30) Volovik, M. V.; Denieva, Z. G.; Gifer, P. K.; Rakitina, M. A.; Batishchev, O. V. Membrane Activity and Viroporin Assembly for the SARS-CoV-2 E Protein Are Regulated by Cholesterol. *Biomolecules* **2024**, *14* (9). DOI: 10.3390/biom14091061 From NLM Medline.

(31) Gopalakrishna, R.; Anderson, W. B. Ca2+-induced hydrophobic site on calmodulin: application for purification of calmodulin by phenyl-Sepharose affinity chromatography. *Biochem Biophys Res Commun* **1982**, *104* (2), 830-836. DOI: 10.1016/0006-291x(82)90712-4 From NLM Medline.

(32) Sahu, I. D.; Lorigan, G. A. Site-Directed Spin Labeling EPR for Studying Membrane Proteins. *Biomed Res Int* **2018**, *2018*, 3248289. DOI: 10.1155/2018/3248289 From NLM Medline.

(33) Schultz, K. M.; Klug, C. S. Use of Site-Directed Spin Labeling EPR Spectroscopy to Study Protein-LPS Interactions. *Methods Mol Biol* **2022**, *2548*, 83-96. DOI: 10.1007/978-1-0716-2581-1_6 From NLM Medline.

(34) Georgieva, E. R. Nanoscale lipid membrane mimetics in spin-labeling and electron paramagnetic resonance spectroscopy studies of protein structure and function. *Nanotechnol Rev* **2017**, *6* (1), 75-92. DOI: 10.1515/ntrev-2016-0080.

(35) Cooper, R. S.; Georgieva, E. R.; Borbat, P. P.; Freed, J. H.; Heldwein, E. E. Structural basis for membrane anchoring and fusion regulation of the herpes simplex virus fusogen gB. *Nat Struct Mol Biol* **2018**, *25* (5), 416-424. DOI: 10.1038/s41594-018-0060-6 From NLM Medline.

(36) Schmidt, T.; Walti, M. A.; Baber, J. L.; Hustedt, E. J.; Clore, G. M. Long Distance Measurements up to 160 A in the GroEL Tetradecamer Using Q-Band DEER EPR Spectroscopy. *Angew Chem Int Ed Engl* **2016**, *55* (51), 15905-15909. DOI: 10.1002/anie.201609617 From NLM Medline.

(37) Georgieva, E. R.; Ramlall, T. F.; Borbat, P. P.; Freed, J. H.; Eliezer, D. The lipid-binding domain of wild type and mutant alpha-synuclein: compactness and interconversion between the broken and extended helix forms. *J Biol Chem* **2010**, *285* (36), 28261-28274. DOI: 10.1074/jbc.M110.157214 From NLM Medline.

(38) Borbat, P. P.; Georgieva, E. R.; Freed, J. H. Improved Sensitivity for Long-Distance Measurements in Biomolecules: Five-Pulse Double Electron-Electron Resonance. *Journal of Physical Chemistry Letters* **2013**, *4* (1), 170-175. DOI: 10.1021/jz301788n.

(39) Borbat, P. P.; Crepeau, R. H.; Freed, J. H. Multifrequency two-dimensional Fourier transform ESR: an X/Ku-band spectrometer. *J Magn Reson* **1997**, *127* (2), 155-167. DOI: S1090-7807(97)91201-5 [pii]

10.1006/jmre.1997.1201.

(40) Jeschke, G.; Polyhach, Y. Distance measurements on spin-labelled biomacromolecules by pulsed electron paramagnetic resonance. *Physical Chemistry Chemical Physics* **2007**, *9* (16), 1895-1910. DOI: 10.1039/b614920k.

(41) Gamliel, D.; Freed, J. H. THEORY OF 2-DIMENSIONAL ESR WITH NUCLEAR MODULATION. *Journal of Magnetic Resonance* **1990**, *89* (1), 60-93. DOI: 10.1016/0022-2364(90)90162-3.

(42) Borbat, P. P.; Freed, J. H. Pulse Dipolar ESR: Distance Measurements. In *Structure and Bonding*, Vol. 152; Springer, 2014; pp 1-82.

(43) Tang, S. G.; Henne, W. M.; Borbat, P. P.; Buchkovich, N. J.; Freed, J. H.; Mao, Y. X.; Fromme, J. C.; Emr, S. D. Structural basis for activation, assembly and membrane binding of ESCRT-III Snf7 filaments. *eLife* **2015**, *4*, Article. DOI: e12548

10.7554/eLife.12548.

(44) Chiang, Y. W.; Borbat, P. P.; Freed, J. H. The determination of pair distance distributions by pulsed ESR using Tikhonov regularization. *J Magn Reson* **2005**, *172* (2), 279-295. DOI: 10.1016/j.jmr.2004.10.012 From NLM Medline.

(45) Srivastava, M.; Georgieva, E. R.; Freed, J. H. A New Wavelet Denoising Method for Experimental Time-Domain Signals: Pulsed Dipolar Electron Spin Resonance. *J Phys Chem A* **2017**, *121* (12), 2452-2465. DOI: 10.1021/acs.jpca.7b00183 From NLM PubMed-not-MEDLINE.

(46) Srivastava, M.; Freed, J. H. Singular Value Decomposition Method to Determine Distance Distributions in Pulsed Dipolar Electron Spin Resonance. *J Phys Chem Lett* **2017**, *8* (22), 5648-5655. DOI: 10.1021/acs.jpclett.7b02379 From NLM PubMed-not-MEDLINE.

(47) Chiang, Y. W.; Borbat, P. P.; Freed, J. H. Maximum entropy: a complement to Tikhonov regularization for determination of pair distance distributions by pulsed ESR. *J Magn Reson* **2005**, *177* (2), 184-196. DOI: 10.1016/j.jmr.2005.07.021 From NLM Medline.